Structure-based Discovery of Novel Ligands for the Orexin 2 Receptor

Jakub Gunera[a], Jillian G. Baker[b], Niek van Hilten[a], Daniel M. Rosenbaum[c] and Peter Kolb[a,]*

[a] Department of Pharmaceutical Chemistry, Philipps-University, Marburg, Hesse, 35032, Germany
[b] Cell Signalling, School of Life Sciences, Queen's Medical Centre, University of Nottingham, Nottingham NG7 2UH, U. K.
[c] Departments of Biophysics and Biochemistry, UT Southwestern Medical Center, Dallas, Texas 75390-8816, U. S. A.

KEYWORDS: Orexin receptor, virtual screening, G Protein-Coupled Receptor, Docking

Abstract

The orexin receptors are peptide-sensing G protein-coupled receptors that are intimately linked with regulation of the sleep/wake cycle. We used a recently solved X-ray structure of the orexin receptor subtype 2 in computational docking calculations with the aim to identify additional ligands with unprecedented chemotypes. We found validated ligands with a high hit rate of 29% out of those tested, none of them showing selectivity with respect to the orexin receptor subtype 1. Furthermore, of the higher-affinity compounds examined, none showed any agonist activity. While novel chemical structures can thus be found, selectivity is a challenge owing to the largely identical binding pockets.

Introduction

The sleep/wake cycle is one of the fundamental features of organisms with a central nervous system. Especially in humans, it guides our every-day lives and is one of the key activities that keep us healthy and sane. Both sleep deprivation and the inability to sleep (insomnia) are therefore unpleasant for an individual and have been shown to have harmful physiological effects (*1*), and constitute a huge burden on society as a whole. (*2*) In order to ameliorate insomnia, two ways can be envisioned: one is to make the brain artificially sleepy; the other is to block the signals that mediate wakefulness. While more traditional insomnia medications have tried to do the former, the latter seems like a strategy that should lead to fewer side effects.

In humans, one of the main pathways to transmit wakefulness signals is the orexin peptide/orexin receptor system. (*3*) It consists of two peptides, orexin A and orexin B, and two G protein-coupled receptors (GPCRs), orexin receptor subtype 1 (OX_1R) and subtype 2 (OX_2R). The two peptides are 33 and 28 amino acids in length, respectively, and bind with nanomolar affinities to both receptors. At the same time, the two receptors are highly homologous, with 63% sequence identity, and, most importantly, differ by only two amino

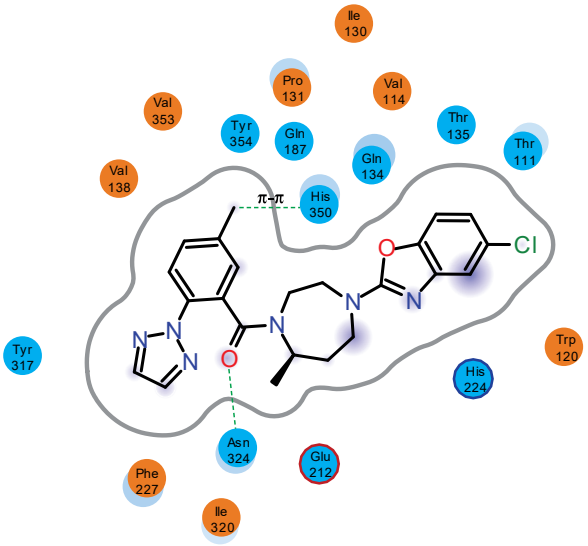

Figure 1: Two-dimensional representation of the binding mode of suvorexant (PDB code 4S0V) generated with the MOE suite. Two interactions of suvorexant with OX_2R are indicated as dashed green lines: An H-bond between amide carbonyl and Asn324$^{6.55}$ and a π-π interaction between 5-methyl-2-triazol-phenyl and His350$^{7.39}$.

acid substitutions in the binding pocket. Despite this high sequence similarity, orexin A achieves a certain amount of selectivity for OX_1R over OX_2R. (*4*)

In 2014, the first antagonist of the OX_2R, suvorexant, obtained regulatory approval as an insomnia medication in the US. One year later, the crystal structure of this molecule in complex with OX_2R was published. (*5*) It showed that suvorexant was binding in a "horseshoe shape", which is consistent with earlier NMR investigations showing that suvorexant was able to adopt such a conformation in solution. (*6*) The receptor was confirmed to be a typical GPCR with seven membrane-spanning helices. Moreover, the crystallographic data demonstrated that suvorexant was interacting with the receptor mainly through hydrophobic interactions. In fact, there are only two polar interactions, one a direct hydrogen bond to Asn324$^{6.55}$, the other a water-mediated hydrogen bond with His350$^{7.39}$ (**Figure 1**). (*5*)

Aiming to exploit this structure in an unbiased computational screen, we have asked three questions. Firstly, could an unbiased docking screen and the analysis of the predicted binding modes suggest other polar interaction possibilities for small molecules in the binding pocket? Secondly, could an apolar binding pocket as this one be as suitable for docking (manifested by high hit rates) as the more polar pockets of the aminergic receptors investigated earlier. (*7*,*8*,*9*,*10*,*11*) Lastly, could comparison of our hit molecules with the already known chemical space for the orexin receptors identify novel chemotypes that might present scaffolds worthwhile to elaborate on further with medicinal chemistry?

Results

Selection of parent hits: Primary docking screen

Docking of 7.337 million compounds from the DrugsNow subset of the ZINC database into the OX_2R (see Methods for details) and subsequent post-processing of its outcome resulted in 6500 unique poses, split up in 6000 from the top ranks of the lists sorted according to HYBRID, DSX, or SZYBKI scores and an additional 500 from the calculations with DOCK. The visual inspection of these poses resulted in 85 virtual hit candidates (HYBRID: 14; DSX: 25; SZYBKI: 14 and DOCK: 32 poses, respectively [**Figure 2**]). Forty-three compounds were available from their vendors and analyzed pharmacologically. These compounds will be referred to as the "parent" compounds **P1**-**P43** in the following and are shown in Table S2, with selected compounds also displayed in **Figure 4**.

Validation of cell lines and examination of primary docking screen

Pharmacological studies were conducted in CHO cells stably expressing the human orexin 1 receptor (CHO-OX_1) or human orexin 2 receptor (CHO-OX_2). Suvorexant, a known dual OX_1/OX_2 receptor antagonist, inhibited the specific binding of both ^{3}H-SB674042 to the human OX_1R and ^{3}H-EMPA to the human OX_2R with high affinity (p K_i 8.51 and 8.53, respectively [**Table 1**]). The known OX_1R antagonists SB334867 and SB674042 were

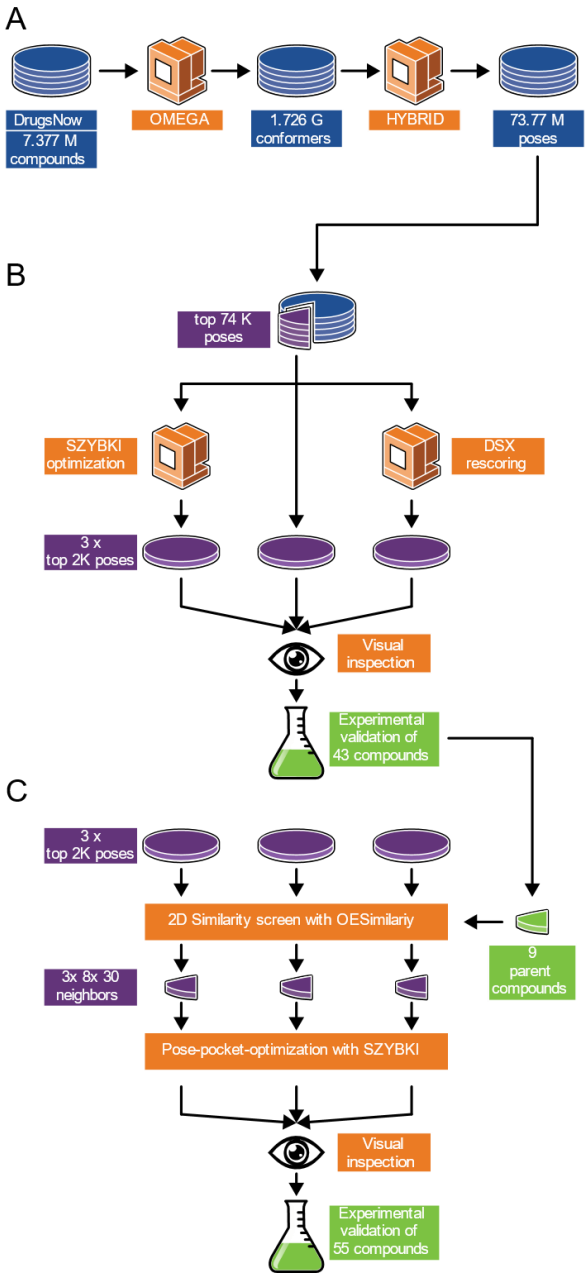

Figure 2: Schematic of the primary docking screen workflow. **A:** The ZINC DrugsNow subset of ~7.4 M compounds was subjected to conformer generation used for docking. In addition, ~4 M ZINC LeadLike compounds were docked as-is. **B:** Threefold post-processing of the top 1 % slice (6500 poses – 2000 each from HYBRID, DSX, SZYBKI and 500 from DOCK) concluded by visual inspection, selection of compounds and their experimental validation. **C:** Schematic of the secondary similarity screen workflow. Eight experimentally validated hits were used as queries for a fingerprint-based similarity screen of three 2000 slices from the primary screen. The three sets of 30 nearest neighbors each were optimized with SZYBKI and subjected to visual inspection. Selected virtual hits were validated experimentally.

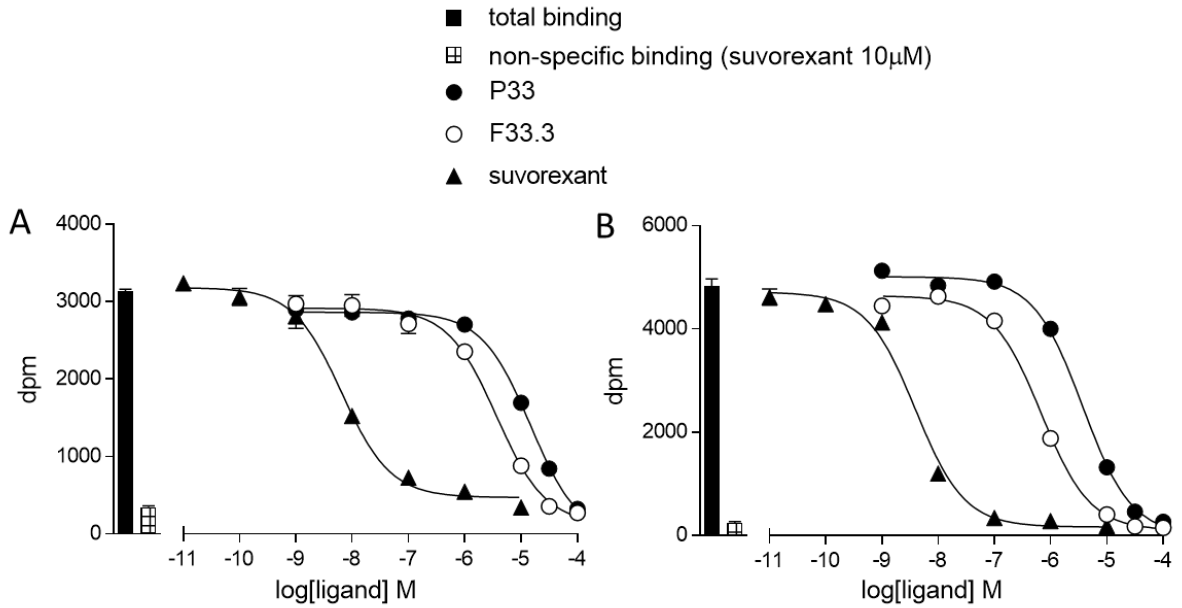

Figure 3: Inhibition of **A** ^{3}H-SB67404 binding to CHO-OX_1 cells and **B** ^{3}H-EMPA binding to CHO-OX_2 cells in response to **P33**, **F33.3** and suvorexant. Bars represent total and non-specific binding (as determined by 10 μM suvorexant) and data point are mean ± sem of triplicate determinations. These experiments are representative of 4 separate experiments. The concentration of radioligand in these experiments was **A:** 1.14 and **B:** 0.60 nM.

found to have much higher affinity for the CHO-OX_1 cells than the CHO-OX_2 cells, whereas the known OX_2R antagonists JNJ10397049 and EMPA had much higher affinity for the CHO-OX_2 cells (**Table 1**). These are consistent with previous values and demonstrate the existence of each of the receptors in the two respective cell lines. (*12*,*13*,*14*) Conversely, in cells not transfected with either receptor, no binding of ^{3}H-SB674042 or ^{3}H-EMPA, respectively, could be observed.

Of the 43 initial compounds identified from the primary docking screen, eleven had some degree of measurable affinity for either the OX_1 or OX_2 receptor, giving an initial hit rate of 26 %. Of these, **P33** had the highest affinity with a pK_i value of 5.54 at the OX_2R (**Figure 3**, **Table 1**, **Figure 4**, for space reasons, all other compounds that are not among the ten with the highest affinity are depicted in the Supplementary Information [**Table S 2**]). Almost all measured compounds did not show selectivity. Five compounds showed a very minor degree of selectivity: **P34** had a 5-fold OX_2R selectivity (ΔpK_i of -0.69), **P9** and **P33** a 4-fold OX_2R selectivity (a ΔpK_i of -0.62 and -0.59, respectively) whilst **P12** and **P18** had at least a 3-fold OX_1R selectivity.

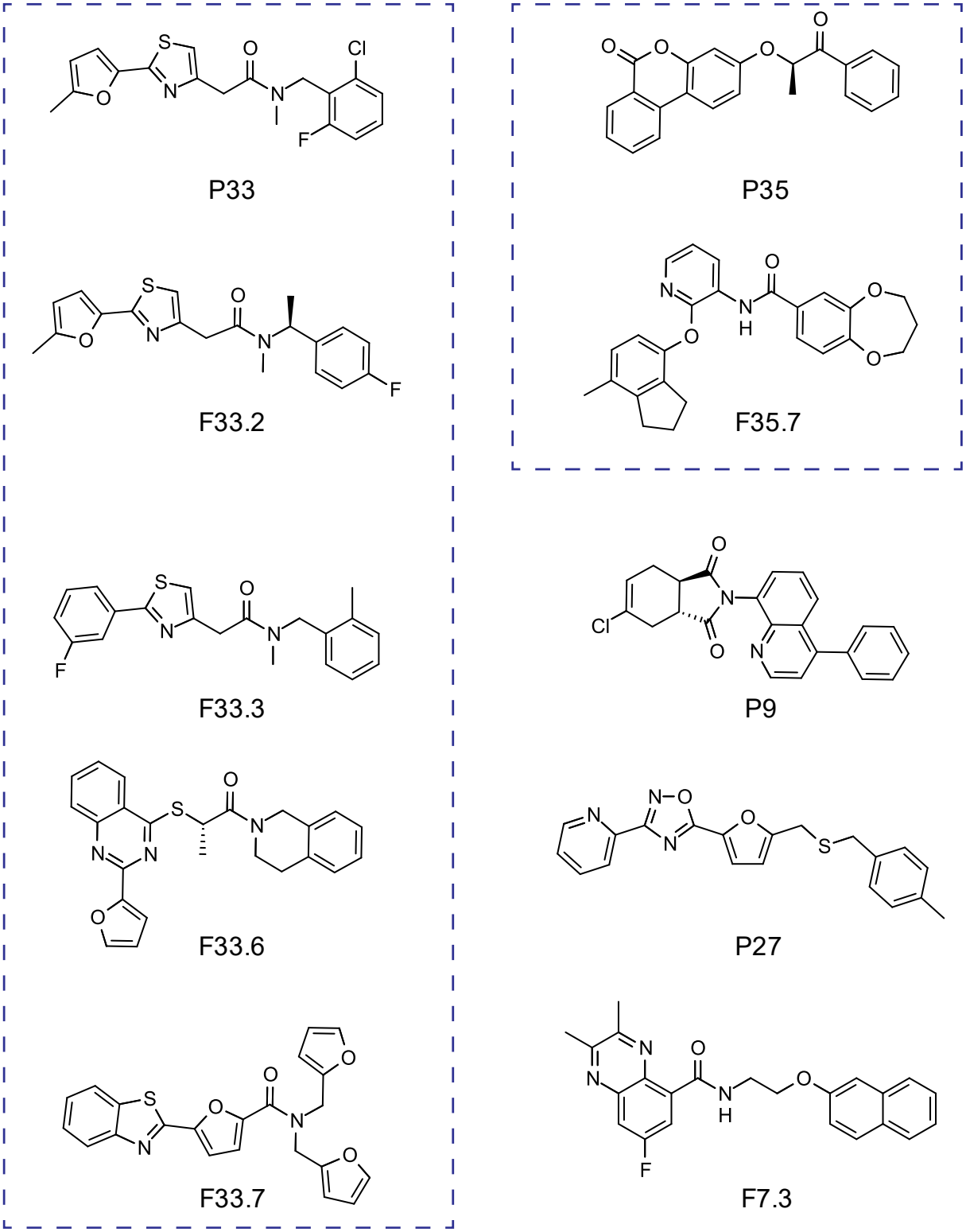

Figure 4: The ten compounds with the highest measured affinity in the ^{3}H-EMPA binding assay to CHO-OX$_2$ cells identified in this study. **P33** and **P35** compound families are emphasized with a box.

Examination of daughter compounds

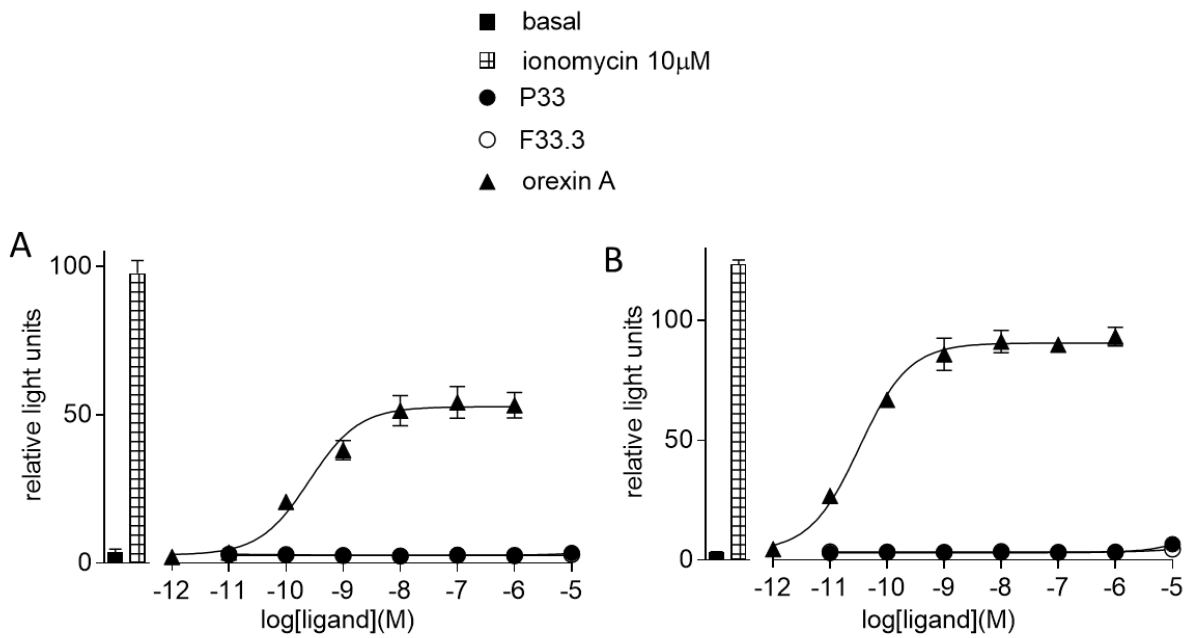

Figure 5: Intracellular calcium release in **A** CHO-OX_1 cells and **B** CHO-OX_2 cells in response to orexin A, **P33** and **F33.3**. Bars represent basal intracellular calcium release and that in response to 10μ M ionomycin alone. Data points are mean ± sem of triplicate determinations and these single experiments are representative of 4 separate experiments in each case.

For nine parent compounds, daughter derivatives (F) were obtained: We selected between one (**P22** and **P31**) and 15 (**P35**) daughter molecules from each parent – in total 54 compounds – based on availability of similar compounds and their favorable docking scores and poses. The identifiers of the daughter compounds in this text are based on the ID of the parent compound and the order number of each of them, separated by a point. E.g. compound **F33.1** is the first daughter compound of parent **P33**. **Table 2** shows their affinities measured against OX_1R and OX_2R. Compound **P33** can be considered the most fruitful parent compound, as all but one of the seven derivatives measured also showed measurable affinity against the OX_2R. Moreover, its daughter **F33.3** bound with the highest affinity of all ligands, at a pK_i of 6.18 (K_i of 660 nM, **Figure 3**). In total, 16 of the 54 derivatives tested bound to the receptor. This brings the hit rate of daughter compounds to 30 %. Finally, to further exclude any non-orexin receptor mediated effects, the most potent ligands were examined for their ability to bind to an unrelated receptor, the human β_1-adrenergic receptor. Although the β_1-antagonist CGP20712A inhibited specific binding with high affinity, none of the ligands with orexin receptor affinity had any detectable binding for the β_1-adrenergic receptor (see supplementary data).

1.1 Examination of functional responses

Orexin 1 and 2 receptors are both G_q-coupled GPCRs and therefore stimulate an increase in intracellular calcium release. To examine whether the compounds had an agonist activity, the ability of some of the higher affinity compounds to stimulate intracellular calcium release was measured. Orexin A stimulated a potent agonist response in both the CHO-OX_1 cells (pEC_{50} 9.67 ± 0.13, 19.4 ± 24 fold over basal, 58.8 ± 2.4 % that of 10 μM ionomycin, n=5) and the CHO-OX_2 cells (pEC_{50} 10.31 ± 0.07, 32.8 ± 4.2 fold over

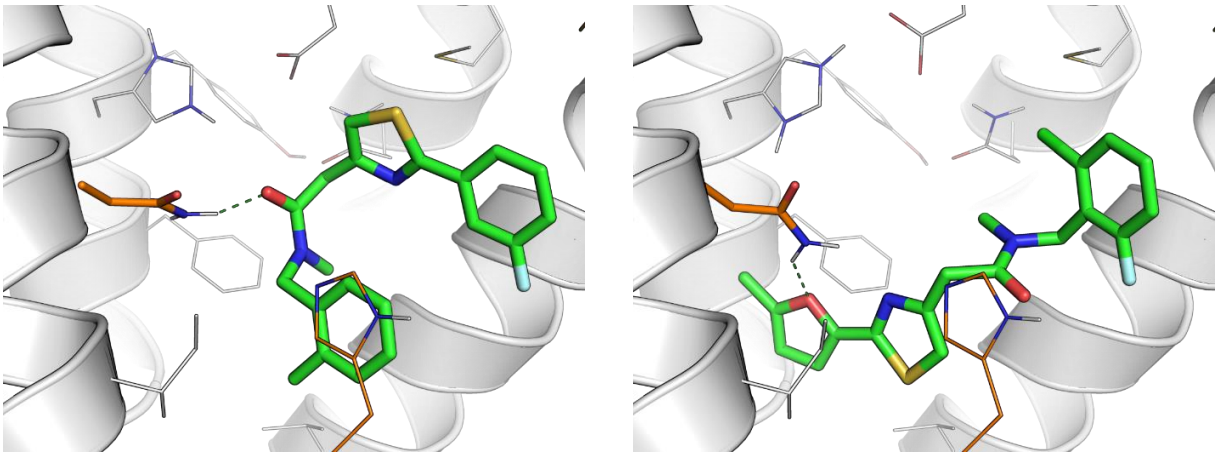

Figure 6: Depictions of **F33.3** (left) and **P33** (right) showing poses of the most potent and the most OX_2R selective compound, respectively. Compounds are shown in green sticks. $Asn324^{6.55}$ and $His350^{7.39}$ in orange sticks (bold and thin, respectively). Helix 7 was removed for clarity. Color code: C green, N blue, O red, S yellow, Cl dark green, F cyan. PDB code: 4S0V.

basal, 71.8 ± 1.8 % that of 10 µM ionomycin, n=6; **Figure 5**). No agonist response was seen in response to any of the other ligands examined. Thus, no agonist response was seen to parent compounds **P9**, **P33** or **P35** or daughter compounds **F7.3**, **F33.2**, **F33.3**, **F33.6**, **F33.7**, or **S2.7** (n=3 to 9 for each ligand at each receptor; **Figure 5**). In addition, no response was seen to parent compounds **P7**, **P21**, **P22**, **P27**, **P32**, **P34**, or daughter compounds **F7.1**, **F21.1**, **F27.2**, **F27.3** at the OX_2R (n=5). Therefore, these compounds, including the highest affinity parent compound (**P33**) and derivative (**F33.3**) had no agonist activity and thus are antagonists at the human OX_1 and OX_2 receptors.

Structure-Activity Relationship

The lack of polar features in the binding pocket is echoed in the ligands. Therefore, it is challenging to develop a clear-cut SAR for them. There are many chemical solutions for a molecule to form favorable interactions with this receptor. In particular, apolar interactions are relatively tolerant towards subtle geometric changes. This tolerance can be seen here as several bulky substituents had very little effect of affinity.

Looking at **P33** and its derivatives (**F33.1**, **F33.2**, **F33.3**, [**F33.4**: no affinity], **F33.5**, **F33.6**, and **F33.7**), all these points are confirmed. This mini-series consists of the most potent parent **P33** and daughter molecule (**F33.3**) with the highest number of active daughter compounds (six). The only polar interaction these molecules form is with $Asn324^{6.55}$, yet the overall binding mode of **P33** is not suvorexant-like (**Figure 6** right). The daughters tell us that the position or existence of the halogens on the benzene rings are not important (**F33.2** and **F33.3** bind), but that more bulk in this region is not favorable (**F33.1** is worse). There seems to be more space around the methyl-furane, however, as it can be replaced with bulkier groups (**F33.6**, **F33.7**). For these latter molecules, a more suvorexant-like binding mode is conceivable. Interestingly, all the most active compounds show a double acceptor feature, which is absent in the weaker ligands. The most potent compound of this series, **F33.3**, might also be the only one truly capable of adapting a suvorexant-like conformation according to docking (**Figure 6** left).

For **P7** and similar (**F7.1**, [**F7.2**: no affinity], **F7.3**, **F7.4**, [**F7.5** and **F7.6**: no affinity], and **F7.7**), a slightly different picture

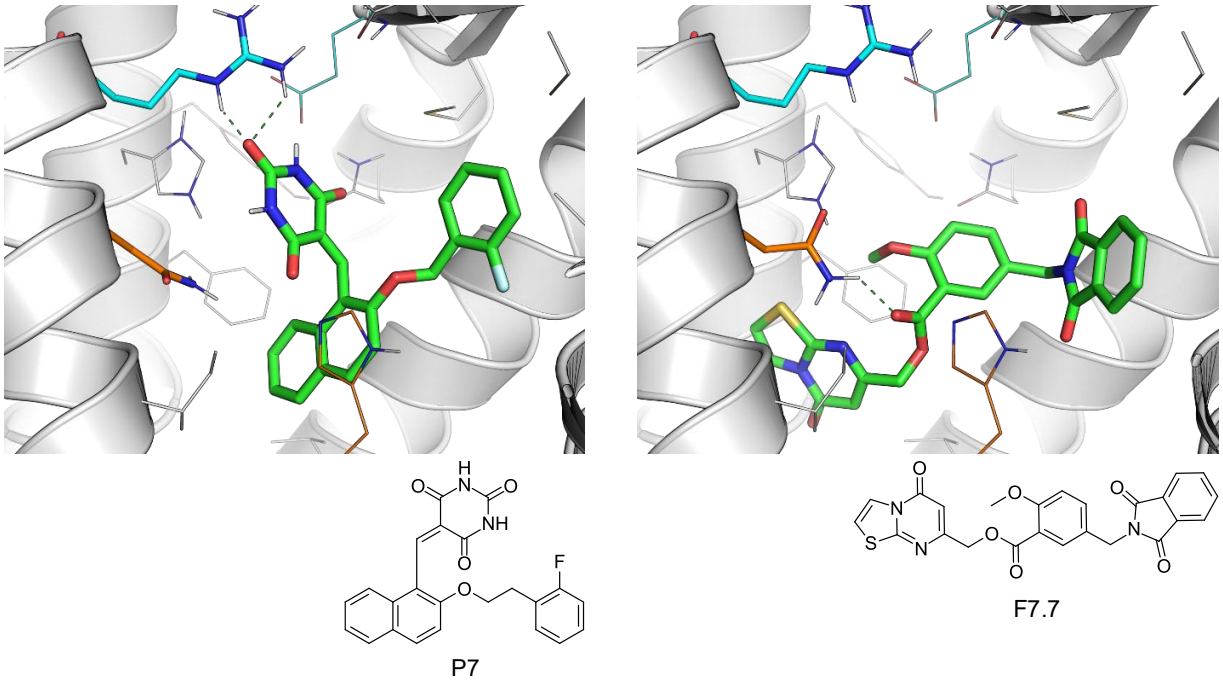

Figure 7: Depictions of poses of **P7** (left) and **F7.7** (right), respectively. Compounds are shown in green sticks. Asn324$^{6.55}$ and His350$^{7.39}$ in orange sticks (bold and thin, respectively). Glu212$^{45.52}$ and Arg328$^{6.59}$ in cyan sticks (bold and thin, respectively). Helix 7 was removed for clarity. Color code: C green, N blue, O red, S yellow, Cl dark green, F cyan. The protein is PDB code: 4S0V.

emerges. Compound **P7** interacts with residues Glu212$^{45.52}$ and Arg328$^{6.59}$, both located at the entrance of the binding site and forming a lid, shielding it from bulk solvent. The derivatives are only bound to Asn324$^{6.55}$. Of note, **F7.7** binds in an orientation reminiscent of a reverse suvorexant binding mode (**Figure 7**). Despite a certain difference in the overall layout, all of the compounds with affinity feature a pyrimidinone ring and a relatively apolar double ring system.

Finally, as a negative example, we turn to parent compound **P9**. Although **P9** has affinity for orexin receptors, none of the 12 derivatives showed much binding. This series also shows the perils of similarity searches, as several of the ligands would not be considered similar by a chemist. Yet, these seemed to interact favorably with the binding pocket in docking. **F9.8** is the only compound with a similar "double lactam" cyclohexene ring and the only to show some effect.

Overall, our docking screen showed that even for relatively featureless apolar binding pockets, ligands can be found in large databases based on shape complementarity (see **Figure 4** for the ten most affine compounds found in this study). Interestingly, the scarcity of strong polar or even charge-charge interaction possibilities did not hamper docking's ability to find ligands, evident from the overall hit rate of 29%, which compares favorably with other studies on class A GPCRs. Several novel chemotypes were identified and might serve as seeds for further development.

Discussion and conclusions

Our unbiased docking screen (using the OX_2R crystal structure) answers the three questions posed in the introduction. A metric that is often used as the figure of merit in a docking screen is the hit rate, defined as the percentage of all tested molecules that are

found to interact with the receptor. In this study, taking the hits from the parent and daughter screen into account, a hit rate of 29% was achieved in the CHO-OX_2 cells, based on binding affinity. Despite the challenging nature of the binding pocket, with only few polar interactions sprinkled throughout, this puts the present screen in the same league as previous studies with polar or even charged features within the binding pockets. Docking itself thus does not seem to be hampered by this comparative scarcity of directional interactions in the OX_2R. The hit rates of the daughter generation are almost the same as the parents' rates, however. This might be because the similarity calculations were based on global similarities. A stricter similarity search, retaining the scaffolds of the parent compounds, might have produced higher hit rates.

Secondly, we took a closer look at the predicted binding modes and compared them with the ones of suvorexant and SB-674042. The majority of molecules interact with very similar residues, predominantly Asn324$^{6.55}$ and His350$^{7.39}$. Interestingly, however, a few of them also formed interactions with Thr111$^{2.61}$, a residue that differs in OX_1R, where it is a serine (Ser103$^{2.61}$). Despite this being a small deviation, such compounds might be starting points for selective orexin receptor antagonists (SORAs). On top of this, compound **P22** forms a hydrogen bond with the backbone carbonyl of Pro131$^{3.29}$, which has so far not been observed in any of the crystal structures.

Lastly, this docking strategy has managed to identify several scaffolds that can be considered novel by common chemoinformatic criteria. Among them are compound **P27**, whose ECFP4 Tanimoto similarity to its closest match amongst any known ligands of OX_2R is only 0.237 (median similarity of 0.115). Two additional compounds, **F33.2** and **F7.4**, show also distant closest matches and low maximum similarities of 0.241 (median of 0.124) and 0.254 (median of 0.121), respectively. In total, 52 compounds that show some affinity in our assay, had an ECFP4 Tanimoto similarity to their closest neighbors of 0.45 or less, and 22 with a similarity value of 0.30 and less, commonly regarded as a threshold indicating dissimilarity (ECFP4 Tanimoto similarity values and ROCS TanimotoCombo scores can be found in the Supplementary Information [**Table S 3** and **Table S 5**]).

A key question for future investigations is whether these scaffolds can easily be derivatized. To answer this question, the composition was analyzed with the PINGUI (*15*) toolbox, which we have developed earlier. Each of the compounds shows a facile synthetic breaking point, yielding fragments of a size that is frequently occurring in building block databases. The number of applicable reactions to fragments of our hits after their retrosynthetical decomposition ranges from two (**F21.3**) to nine (**P18**) (**Table S 6**). It is likely that also the derivatives will show affinity, as we have already exhausted existing chemical space through SAR-by-catalog. In particular compound **P33** seems very promising, as five of its daughter compounds (**F33.1-3**, **F33.6** and **F33.7**) also show binding to the receptor. Our analysis found 103 retrosynthetical disconnections. Four unique reactions can be applied to the resulting fragment set. It has to be noted that **P33** shares some moieties with the known ligands EMPA and SB-649868. Based on our SAR considerations and our experience from similar projects (*15*,*16*) we are convinced that there is room for diversity around the common rings, however.

By way of better characterization, we also tested our compounds against the OX_1R, despite the fact that we never made a prediction about selectivity. Not unexpectedly, most of the compounds behave as DORAs. In fact, our OX_2R-focused docking produced five compounds with a measurable affinity selectivity between OX_2R and OX_1R, but only

up to a maximum selectivity of 5-fold (a ΔpK_i of 0.6). Although measurable, these values are low and at the detection limit of the assay. At the same time, OX2R-selective compounds are generally regarded as preferable for the treatment of insomnia, as they carry lower risks of OX1R-mediated side effects, such as compulsive behavior and substance misuse disorders. (*17*)

Would this be different if we had docked to both subtypes? In order to answer this question, we did a dual docking as described before. (*11*) Briefly, the same small molecule dataset was docked to both the OX_1R and the OX_2R. For the OX_1R, the X-ray structure with PDB ID 4ZJ8 (*18*) was used and prepared in an identical fashion as its OX_2R counterpart. After docking, molecules were reranked in order to favor molecules that would display the desired selectivity. (*11*) The molecules populating the top 500 ranks of this docking were all distinct from the ones of the original docking against the OX2R, and, therefore, there was also no overlap between the sets of assayed molecules. However, even with this differential docking, we did not find ligands with more than a ΔpK_i of 0.5. The data for these molecules is presented in **Table 3**. It thus stands to reason that this featureless binding pocket presents a case where standard docking protocols run in high-throughput mode do not discriminate well enough in order to predict selectivity between the two orexin receptor subtypes. As we have shown recently, this is different for dedicated more precise docking calculations used to optimize ligand selectivity, driving it towards higher OX_1R affinity. (*19*)

In summary, our *in silico* screen yielded several compounds with potential for further development as orexin receptor ligands and shed light on possible alternative interaction patterns that can be exploited in future screening and optimization work.

Experimental Section

Receptor preparation

The crystal structure of the OX_2R liganded by suvorexant (PDB code 4S0V) (*5*) was prepared using the MOE software suite. (*20*) Briefly, i) all water molecules, metal ions, precipitants and lipids were removed. ii) The fusion protein glycogen synthase from *P. abysii* was cleaved from the receptor at amino acids $Lys294^{6.25}$ and $Gln254^{5.69}$. iii) Loop breaks and fusion protein cleavage sites were capped with methylamine and acetyl at C- and N-termini, respectively. iv) Hydrogen atoms were added, and the protonation states of titratable amino acids were assigned using MOE's Protein Preparation subroutines (pH-value 7.4, temperature 300 K). Protonation states of histidines and rotamers of head groups of glutamines and asparagines were visually inspected and adjusted according to their protein environment.

Database generation

The DrugsNow subset of the ZINC database (*21*) was downloaded as SMILES strings (7.377 million entries). The subset was split into batches of 10000 molecules (738 batches). Each batch was submitted to OpenEye's OMEGA program for conformer generation. (*22*) For each molecular entity, a maximum number of 400 conformers was generated. The energy window parameter was set to 10.0 and the rms (root mean square deviation of conformer coordinates) parameter to 0.5. The "strict" flag was set to "true" ensuring that molecules without fully specified stereochemistry were discarded. A total of 1.726 billion conformers were generated. For docking with DOCK, the ZINC LeadLike subset was downloaded in flexibase format (3.987 million entries) and used as-is (**Figure 2**A).

Docking

Docking was performed using OpenEye's HYBRID program. (*23*,*24*) The ensemble of conformations of each molecule was overlaid

with the co-crystallized ligand (suvorexant) in order to determine the best suited conformer for the following exhaustive docking. The method for overlaying conformers is built directly into the HYBRID engine and is based on the same methodology as implemented in the OEChem API and the ROCS application. (*25*) For the actual docking step – translational and rotational optimization of a compound conformer within the binding site of the protein – HYBRID scores for a given protein-ligand complex were calculated based on the shape and electrostatic complementarity of the ligand and the protein's binding site. Shape and electrostatic features are represented by Gaussian potentials. During optimization, the overlap between ligand and protein features is maximized. After docking, the 100 best-scored poses were extracted from each batch and aggregated into one sorted scoring list (73800, entries, corresponds to best scored percentile of the entire docking run).

The ZINC LeadLike subset was docked with DOCK. (*26*) Briefly, molecules were placed using guiding points inside the pocket that had been derived from suvorexant bound to the OX_2R in the crystal structure (PDB code 4S0V) (*5*).

All docking scores can be found in the supplementary information (**Table S 4**). Molecules were purchased from various vendors, as listed in Table S2. Purity of all ligands is ≥ 95 %, as determined by LC/MS and different methods employed by the vendors.

Post-processing

The scoring list of ~74000 poses was treated in three different ways: i) left unchanged (sorted by HYBRID score), ii) rescored by DSX (*27*) and iii) submitted to a rigid body optimization procedure using OpenEye's SZYBKI program. (*28*) During this optimization process, the atoms of the receptor were kept fixed at their crystallographic positions, while the rotational, translational and torsional degrees of freedom of each pose were optimized using a Poisson-Boltzmann solvation model. The resulting poses were sorted by the SZYBKI ligand-protein interaction energy.

From each of the scoring lists (HYBRID, DSX and SZYBKI), a slice of 2000 poses was extracted and subjected to visual inspection in order to remove those that form improbable interactions that are not sufficiently penalized by present-day scoring functions. In addition, the 500 best-scored poses from the docking run with DOCK were added to the visual inspection. Selected compounds were acquired from their respective vendors and analyzed pharmacologically. Parent generation of compounds are denoted with a capital **P** (**Figure 2**B).

Similarity screen

Several experimentally validated compounds from the parent generation (both with and without affinity against the receptor) were used as queries for the retrieval of close analogs by a fingerprint-based similarity screen: For each of the nine hits (**P7**, **P9**, **P21**, **P22**, **P27**, **P31**, **P32**, **P33** and **P35**), the 30 nearest neighbors were retrieved from the three 2000 entries-long slices (HYBRID, DSX and SZYBKI [**Figure 2**B]). The retrieved poses were all subjected to optimization with SZYBKI. The resulting geometries were visually inspected and the selected compounds were acquired from their respective vendors and analyzed pharmacologically (daughter generation of compounds denoted with a capital **F**) (**Figure 2**C).

Experimental validation

Materials

^{3}H-SB674042 was from Metis Laboratories (New York, USA) and ^{3}H-EMPA was from Novandi Chemistry (Södertälje, Sweden). Fluo-4AM and pluronic F-127 were

from Invitrogen (Oregon, USA). Orexin A, SB334867, SB674042, JNJ10397049 and EMPA were from Tocris Life Sciences (Avonmouth, UK). Suvorexant was from Selleckchem (Houston, USA). Gibco fetal bovine serum was from Fischer Scientific (Loughborough, UK). All other reagents were from Sigma Aldrich (Poole, UK).

Cell-culture

CHO cells stably expressing either the human OX_1 or OX_2 receptor (originally a gift from Heptares, UK) were secondarily transfected with an SRE-luciferase reporter gene and stable clones selected by dilution cloning to create CHO-OX_1 and CHO-OX_2 stable cell lines. Cells were grown in Dulbecco's modified Eagle's medium nutrient mix F12 (DMEM/F12) containing 10 % fetal calf serum (FCS) and 2 mM L-glutamine in a 37°C humidified 5 % CO_2: 95 % air atmosphere.

Whole cell ^{3}H-radioligand binding

The affinity of compounds for the OX_1 and OX_2 receptors were determined from whole cell binding studies. Experiments were conducted on confluent cells in white-sided 96-well view plates as previously described (2 hour 37°C incubation with radioligand and competing ligand in 200 µl serum-free media, Baker 2005). A 7-point concentration response curve (each point in triplicate) was examined for each ligand in each experiment. Suvorexant (10 µM) was used to define non-specific binding. The affinity of the radioligands has previously been determined as 4.65 nM for ^{3}H-SB674042 in the CHO-OX_1 cells and 7.86 nM for ^{3}H-EMPA in the CHO-OX_2 cells. (*14*) Cells were inspected under a light microscope to ensure they were still present after the 2-hour incubation, both before and after the wash. In a few cases, high concentrations (100µM) of competing ligand caused the cells to round up and be washed off the plates. These concentrations were excluded from the analysis.

The IC_{50} value of competing ligands was determined from a sigmoidal response curve (plotted in Prism 7) where the IC_{50} is the concentration required to inhibit 50 % of the specific binding of the ^{3}H-radioligand, [A] is the concentration of the competing ligand.

$$\%\ specific\ binding = 100 - \frac{100 \cdot [A]}{IC_{50} + [A]}$$

The K_i values for the competing ligands was then determined from the IC_{50} values using Cheng-Prusoff equation where [L] is the concentration of radioligand in that experiment and L_{KD} is the K_D value of the radioligand (as determined from saturation binding (*14*)):

$$K_i = \frac{IC_{50}}{1 + \frac{[L]}{L_{KD}}}$$

Intracellular calcium release

Calcium measurements were made using a Flexstation 3 at 37°C. Cells, seeded into black 96-well view plates, were loaded with Fluo-4AM / pluronic-F127 in serum-free media containing probenecid (25 mM) for 45 minutes at 37°C. Cells were washed with 200 µl HEPES buffered saline (HBS, containing 2 µM $CaCl_2$) per well, before a further 80 µl HBS was then added to each well. Ligands were diluted in HBS to 5 times final concentration in round bottomed 96-well compound plates. During the experiment, the Flexstation robotics added 20 µl of ligand from the compound plate into the existing 80 µl HBS in the cell plate (1:5 dilution in well). Ionomycin (10 µM) and orexin A (1 µM) were used as positive controls each plate in each experiment. Calcium mobilization was followed for 120 seconds and data were plotted as the maximum value obtained for calcium mobilization over the basal value obtained for that well before the addition of ligand.

A sigmoidal concentration response curve was fitted to the data (using Prism 7) where E_{max} is the maximum response, [A] is the

agonist concentration and EC_{50} is the concentration of agonist that produces 50 % of the maximal response:

$$response = \frac{E_{max} \cdot [A]}{EC_{50} + [A]}$$

Associated content

Tabular data as PDF files containing compound structures, SMILES strings, and supplier information; Tanimoto fingerprint similarities, ROCS TanimotoCombo scores, docking scores; and retrosynthetical analysis. Predicted complex structures for all molecules are provided in PDB format.

Author information

Corresponding author

For P.K.: E-mail, peter.kolb@uni-marburg.de

Author contributions

J.G., D.R. and P.K. designed research. J.G. performed docking calculations and selected compounds together with P.K. J.G.B. performed pharmacological assays and analysis. J.G. J.G.B. and P.K. wrote the manuscript.

Funding sources

J.G.'s Ph.D. thesis was funded through the LOEWE Centre Synmikro. J.G.B. was funded by an MRC grant MR/M00032X/1. P.K. thanks the German research foundation DFG for Heisenberg professorship KO4095/4-1.

Acknowledgments

We thank Richard Proudman for technical assistance with the pharmacological assays and Matthäus Drabek for his input during compound selection.

Ancillary Information

Supporting information available: supporting methods and experimental figures, tables of structures and SMILES for each molecule tested in this work, the results of the PAINS analysis and similarities of all ligands against themselves as well as known ligands.

References

1. Bentivoglio, M.; Grassi-Zucconi, G. The pioneering experimental studies on sleep deprivation. *Sleep* **1997,** *20* (7), 570-576.

2. Czeisler, C. A. Impact of sleepiness and sleep deficiency on public health--utility of biomarkers. *J. Clin. Sleep Med.* **2011,** *7* (5 Suppl), S6-S8.

3. Ma, S.; Hangya, B.; Leonard, C. S.; Wisden, W.; Gundlach, A. L. Dual-transmitter systems regulating arousal, attention, learning and memory. *Neurosci. Biobehav. Rev.* **2017,** *85,* 21-33.

4. Sakurai, T.; Yanagisawa, M. Orexins and orexin receptors: a family of hypothalamic neuropeptides and G protein-coupled receptors that regulate feeding behavior. *Cell* **1998,** *92* (4), 573-585.

5. Yin, J.; Mobarec, J. C.; Kolb, P.; Rosenbaum, D. M. Crystal structure of the human OX2 orexin receptor bound to the insomnia drug suvorexant. *Nature* **2015,** *519,* 247-250.

6. Cox, C. D.; McGaughey, G. B.; Bogusky, M. J.; Whitman, D. B.; Ball, R. G.; Winrow, C. J.; Renger, J. J.; Coleman, P. J. Conformational analysis of N,N-disubstituted-1,4-diazepane orexin receptor antagonists and implications for receptor binding. *Bioorg. Med. Chem. Lett.* **2009,** *19* (11), 2997-3001.

7. Kolb, P.; Rosenbaum, D. M.; Irwin, J. J.; Fung, J. J.; Kobilka, B. K.; Shoichet, B. K. Structure-based discovery of β2-adrenergic receptor ligands. *Proc. Natl. Acad. Sci.* **2009,** *106* (16), 6843-6848.

8. Carlsson, J.; Coleman, R. G.; Setola, V.; Irwin, J. J.; Fan, H.; Schlessinger, A.; Sali, A.; Roth, B. L.; Shoichet, B. K. Ligand discovery from a dopamine D3 receptor homology model and crystal structure. *Nat. Chem. Biol.* **2011,** *7,* 769-778.

9. Weiss, D. R.; Ahn, S.; Sassano, M. F.; Kleist, A.; Zhu, X.; Strachan, R.; Roth, B. L.; Lefkowitz, R. J.; Shoichet, B. K. Conformation Guides Molecular Efficacy in Docking Screens of Activated β-2 Adrenergic G Protein Coupled Receptor. *ACS Chem. Biol.* **2013,** *8* (5), 1018-1026.

10. Sabio, M.; Jones, K.; Topiol, S. Use of the X-ray structure of the beta2-adrenergic receptor for drug discovery. Part 2: Identification of active compounds. *Bioorg. Med. Chem. Lett.* **2008,** *18* (20), 5391-5395.

11. Schmidt, D.; Bernat, V.; Brox, R.; Tschammer, N.; Kolb, P. Identifying Modulators of CXC Receptors 3 and 4 with Tailored

Selectivity using Multi-Target Docking. *ACS Chem. Biol.* **2015,** *10,* 715-724.

12. Langmead, C. J.; Jerman, J. C.; Brough, S. J.; Scott, C.; Porter, R. A.; Herdon, H. J. Characterisation of the binding of [3H]-SB-674042, a novel nonpeptide antagonist, to the human orexin-1 receptor. *Br. J. Pharmacol.* **2004,** *141,* 340-346.

13. Malherbe, P.; Borroni, E.; Gobbi, L.; Knust, H.; Nettekoven, M.; Pinard, E.; Roche, O.; Rogers-Evans, M.; Wettstein, J. G.; Moreau, J. L. Biochemical and behavioural characterization of EMPA, a novel high-affinity, selective antagonist for the OX(2) receptor. *Br. J. Pharmacol.* **2009,** *156,* 1326-1341.

14. Proudman, R. G.; Baker, J. G. The affinity and selectivity of orexin A, orexin B and orexin antagonists for the human orexin 1 and orexin 2 receptors, 2018. http://www.pa2online.org. http://www.pa2online.org/abstract/abstract.jsp?abid=33656 (accessed August 30, 2019).

15. Chevillard, F.; Rimmer, H.; Beti, C.; Pardon, E.; Ballet, S.; van Hilten, N.; Steyart, J.; Diederich, W. . E.; Kolb, P. Binding-Site Compatible Fragment Growing Applied to the Design of β2-Adrenergic Receptor Ligands. *J. Med. Chem.* **2018,** *61* (3), 1118-1129.

16. Chevillard, F.; Stotani, S.; Karawajczyk, A.; Hristeva, S.; Pardon, E.; Steyaert, j.; Tzalis, D.; Kolb, P. Interrogating dense ligand chemical space with a forward-synthetic library. *Proc. Natl. Acad. Sci.* **2019,** *116,* 11496-11501.

17. Boss, C.; Roch, C. Recent trends in orexin research—2010 to 2015. *Bioorg. Med. Chem. Lett* **2015,** *25* (15), 2875-2887.

18. Yin, J.; Babaoglu, K.; Brautigam, C. A.; Clark, L.; Shao, Z.; Scheuermann, T. H.; Harrell, C. M.; Gotter, A. L.; Roecker, A. J.; Winrow, C. J.; Renger, J. J.; Coleman, P. J.; Rosenbaum, D. M. Structure and ligand-binding mechanism of the human OX1 and OX2 orexin receptors. *Nat. Struct. Mol. Biol.* **2016,** 293-299.

19. Hellmann, J.; Drabek, M.; Yin, J.; Gunera, J.; Pröll, T.; Kraus, F.; Langmead, C. J.; Hübner, H.; Weikter, D.; Kolb, P.; Rosenbaum, D. M.; Gmeiner, P. Structure-based development of a subtype-selective orexin 1 receptor antagonist. *Proc. Natl. Acad. Sci.* **2020,** *177* (30), 18059-18067.

20. Chemical Computing Group, Inc. Molecular Operating Environment (MOE) 2015.10. *1010 Sheerbrooke St. West, Suite #910, Montreal, QC, Canada, H3A 2R7,* **2015**.

21. Irwin, J. J.; Shoichet, B. K. ZINC - a free database of commercially available compounds for virtual screening. *J. Chem. Inf. Model.* **2005,** *45* (1), 177-182.

22. Hawkins, P. C. D.; Skillman, A. G.; Warren, G. L.; Ellingson, B. A.; Stahl, M. T. Conformer Generation with OMEGA: Algorithm and Validation Using High Quality Structures from the Protein Databank and the Cambridge Structural Database. *J. Chem. Inf. Model.* **2010,** *50* (4), 572-584.

23. McGann, M. FRED Pose Prediction and Virtual Screening Accuracy. *J. Chem. Inf. Model.* **2011,** *51,* 578-596.

24. McGann, M. FRED and HYBRID docking performance on standardized datasets. *J. Comput. Aided Mol. Des.* **2012,** *26,* 897-906.

25. Hawkins, P. C. D.; Skillman, A. G.; Nicholls, A. Comparison of Shape-Matching and Docking as Virtual Screening Tools. *J. Med. Chem.* **2007,** *50,* 74-82.

26. Shoichet, B. K.; Leach, A. R.; Kuntz, I. D. Ligand solvation in molecular docking. *Funct. Genet.* **1999,** *34,* 4-16.

27. Neudert, G.; Klebe, G. DSX: A Knowledge-Based Scoring Function for the Assessment of Protein–Ligand Complexes. *J. Chem. Inf. Model.* **2011,** *51,* 2731–2745.

28. OpenEye Scientific Software, Inc., Sante Fe, NM, USA. http://www.eyesopen.com.

Table of contents graphic

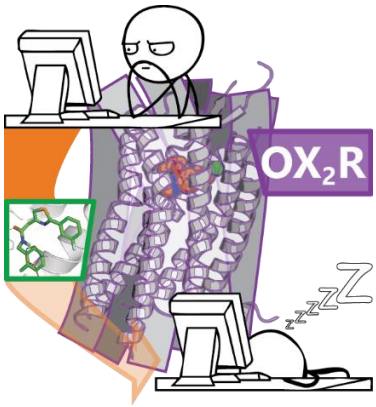

Table 1: pK_i values, obtained for five known orexin ligands and the initial 43 compounds identified from the primary docking screen, from whole cell binding studies as determined from using ^{3}H-SB674042 (CHO-OX_1 cells) and ^{3}H-EMPA (CHO-OX_2 cells). Values are mean ± sem from n separate experiments.

app = apparent K_i value. Here, the maximal achievable concentration of competing ligand was not able to fully inhibit the radioligand specific binding. In cases where greater than 50% specific binding was inhibited, an apparent K_i value is given, assuming that if a greater concentration of ligand were possible, full inhibition of specific binding would have occurred.

IC_{50} > 100 μM. Here, inhibition of specific binding by the competing ligand was less than 50% so an IC_{50} value, and therefore K_i value, could not be calculated. The IC_{50} must therefore have been greater than the maximum concentration of competing.

ep = early plateau. Some ligands did not fully inhibit radioligand binding but appeared to reach an early plateau. Here increasing concentrations of competing ligand reached a maximum inhibition that was less than that achieved by suvorexant (similar to that seen in Proudman and Baker 2018 (*14*)). In these cases, an apparent K_i value is given for the partial inhibition of specific binding. The percentage of specific binding inhibited was 79.2 ± 3.3% for **P27** and 63.7 ± 2.1% for **P35** in the CHO-OX_2 cells.

ID	**CHO-OX_1**		**CHO-OX_2**	
	pK_i	**n**	**pK_i**	**n**
suvorexant	8.51 ± 0.06	13	8.53 ± 0.03	17
SB334867	7.38 ± 0.04	5	5.43 ± 0.08	4
SB674042	8.41 ± 0.08	5	6.70 ± 0.11	3
JNJ10397049	5.87 ± 0.02	5	8.18 ± 0.14	4
EMPA	5.35 ± 0.05	6	8.17 ± 0.05	5
P1	No binding	4	No binding	4
P2	No binding	4	No binding	4
P3	No binding	4	IC_{50} > 100 μM	4
P4	IC_{50} > 100 μM	4	No binding	4
P5	No binding	4	IC_{50} > 100 μM	4
P6	No binding	4	No binding	4
P7	4.48 ± 0.08^{app}	4	4.57 ± 0.10^{app}	5
P8	No binding	3	IC_{50} > 100 μM	4
P9	4.85 ± 0.05^{app}	9	5.40 ± 0.06^{app}	9
P10	IC_{50} > 100 μM	4	IC_{50} > 100 μM	4
P11	No binding	4	No binding	4
P12	4.75 ± 0.09	4	4.21 ± 0.02^{app}	4
P13	IC_{50} > 100 μM	4	4.22 ± 0.03^{app}	4
P14	No binding	4	No binding	4
P15	IC_{50} > 100 μM	4	4.17 ± 0.01^{app}	4
P16	No binding	3	No binding	4
P17	IC_{50} > 100 μM	4	IC_{50} > 100 μM	4

ID	CHO-OX_1		CHO-OX_2	
P18	4.67 ± 0.11^{app}	4	$IC_{50} > 100$ µM	4
P19	$IC_{50} > 100$ µM	4	$IC_{50} > 100$ µM	4
P20	No binding	4	No binding	4
P21	4.36 ± 0.05^{app}	4	4.23 ± 0.03^{app}	5
P22	$IC_{50} > 100$ µM	4	4.49 ± 0.05^{app}	5
P23	No binding	4	No binding	4
P24	$IC_{50} > 100$ µM	4	$IC_{50} > 100$ µM	4
P25	No binding	4	No binding	4
P26	$IC_{50} > 100$ µM	4	$IC_{50} > 100$ µM	4
P27	4.81 ± 0.05	4	5.07 ± 0.03^{ep}	5
P28	No binding	4	$IC_{50} > 100$ µM	4
P29	No binding	4	No binding	4
P30	No binding	4	$IC_{50} > 100$ µM	4
P31	$IC_{50} > 100$ µM	3	$IC_{50} > 100$ µM	4
P32	No binding	4	No binding	5
P33	4.93 ± 0.03	8	5.55 ± 0.02	9
P34	$IC_{50} > 100$ µM	4	4.69 ± 0.02^{app}	4
P35	5.27 ± 0.08	9	5.27 ± 0.06^{ep}	10
P36	No binding	4	No binding	4
P37	$IC_{50} > 100$ µM	4	No binding	4
P38	$IC_{50} > 100$ µM	4	$IC_{50} > 100$ µM	4
P39	No binding	4	No binding	4
P40	$IC_{50} > 100$ µM	4	No binding	4
P41	No binding	9	No binding	9
P42	No binding	4	No binding	4
P43	$IC_{50} > 100$ µM	4	$IC_{50} > 100$ µM	4

Table 2: pK_i values, obtained for parent and daughter compounds from whole cell binding studies as determined from using ^{3}H-SB674042 (CHO-OX_1 cells) and ^{3}H-EMPA (CHO-OX_2 cells). Values are mean ± sem from n separate experiments.

app = apparent K_i value (as above, greater than 50% specific binding was inhibited, so an apparent K_i value is given, assuming that if a greater concentration of ligand were possible, full inhibition of specific binding would have occurred). Where inhibition of specific binding was less than 50%, IC_{50} > concentration of maximum concentration of competing ligand used is given.

ep = early plateau (as above, competing ligand appeared to a plateau whereby increasing competing ligand concentration could not fully inhibit the radioligand. An apparent K_i value is given for the partial inhibition of specific binding. The percentage of specific binding inhibited was 57.2 ± 2.2% for **F7.3**, 52.2 ± 2.2% for **F9.8**, 64.6 ± 3.5% for **F32.2**, and 58.7 ± 4.7% for **F35.7**, respectively, in the CHO-OX_1. In the CHO-OX_2 cells, the percentage of specific binding inhibited was 61.7 ± 4.6% for **F7.3**, 49.9 ± 4.5% for **F9.8**, 39.9 ± 3.5% for **F32.2**, and 67.1 ± 4.6% for **F35.7**, respectively.

ID	CHO-OX_1		CHO-OX_2	
	pK_i	**n**	**p**K_i	**n**
P7	4.48 ± 0.08^{app}	4	4.57 ± 0.10^{app}	5
F7.1	4.68 ± 0.04	4	4.48 ± 0.03^{app}	4
F7.2	No binding	5	No binding	5
F7.3	5.90 ± 0.10^{ep}	5	5.83 ± 0.05^{ep}	5
F7.4	4.83 ± 0.07	5	4.89 ± 0.02	5
F7.5	No binding	5	No binding	5
F7.6	$IC_{50} > 100$ µM	5	$IC_{50} > 100$ µM	5
F7.7	$IC_{50} > 100$ µM	5	4.34 ± 0.06^{app}	5
F7.8	No binding	5	No binding	5
P9	4.85 ± 0.05	9	5.40 ± 0.06	9
F9.1	$IC_{50} > 100$ µM	5	$IC_{50} > 100$ µM	5
F9.2	No binding	5	No binding	5
F9.3	4.49 ± 0.04^{app}	5	$IC_{50} > 100$ µM	5
F9.4	No binding	5	No binding	5
F9.5	No binding	5	No binding	5
F9.6	$IC_{50} > 100$ µM	5	$IC_{50} > 100$ µM	5
F9.7	No binding	5	No binding	5
F9.8	5.11 ± 0.10^{ep}	5	4.97 ± 0.06^{ep}	5
F9.9	$IC_{50} > -5$	5	$IC_{50} > -5$	5
F9.10	No binding	5	No binding	5
F9.11	No binding	5	No binding	5
F9.12	No binding	5	No binding	5
P21	4.36 ± 0.05^{app}	4	4.23 ± 0.03^{app}	5
F21.1[a]	4.83 ± 0.09	4	4.44 ± 0.01^{app}	4
F21.2	No binding	3	No binding	4
F21.3[b]	No binding	4	$IC_{50} > 100$ µM	4
F21.4	$IC_{50} > 100$ µM	4	$IC_{50} > 100$ µM	4
P22	$IC_{50} > 100$ µM	4	4.49 ± 0.05^{app}	5
F22.1[b]	No binding	4	$IC_{50} > 100$ µM	4
P27	4.81 ± 0.05	4	5.07 ± 0.03^{ep}	5
F27.1	No binding	4	$IC_{50} > 100$ µM	4
F27.2	$IC_{50} > 100$ µM	4	4.39 ± 0.05^{app}	4
F27.3	4.82 ± 0.04	4	4.49 ± 0.01^{app}	4
F27.4	No binding	4	No binding	4
F27.5	No binding	4	No binding	4
F27.6	$IC_{50} > 100$ µM	4	4.23 ± 0.05^{app}	4
F27.7	No binding	3	No binding	4
F27.8	No binding	3	No binding	4
P31	$IC_{50} > 100$ µM	3	$IC_{50} > 100$ µM	4

ID	CHO-OX$_1$		CHO-OX$_2$	
F31.1	No binding	5	IC_{50} > 100 μM	4
P32	No binding	4	No binding	5
F32.1	IC_{50} > 100 μM	4	4.22 ± 0.05^{app}	4
F32.2	5.10 ± 0.01^{ep}	4	4.98 ± 0.06^{ep}	4
P33	4.93 ± 0.03	8	5.55 ± 0.02	9
F33.1[b]	4.83 ± 0.09	4	4.44 ± 0.01^{app}	4
F33.2	4.77 ± 0.02	4	5.53 ± 0.05	4
F33.3	5.49 ± 0.05	4	6.18 ± 0.03	4
F33.4	No binding	5	4.27 ± 0.03^{app}	4
F33.5	IC_{50} > 100 μM	4	IC_{50} > 100 μM	4
F33.6	5.05 ± 0.12	4	5.50 ± 0.05	4
F33.7	5.45 ± 0.13	4	5.50 ± 0.02	4
P35	5.27 ± 0.08	9	5.27 ± 0.06^{ep}	10
F35.1	IC_{50} > 100 μM	5	IC_{50} > 100 μM	5
F35.2	No binding	5	No binding	5
F35.3	No binding	5	No binding	5
F35.4	No binding	5	No binding	5
F35.5	No binding	5	No binding	5
F35.6	4.61 ± 0.03^{app}	5	4.38 ± 0.08^{app}	5
F35.7	5.29 ± 0.05^{ep}	5	5.19 ± 0.07^{ep}	5
F35.8	IC_{50} > 100 μM	5	IC_{50} > 100 μM	5
F35.9	IC_{50} > 100 μM	5	IC_{50} > 100 μM	5
F35.10	No binding	5	No binding	5
F35.11	No binding	5	No binding	5
F35.12	No binding	5	No binding	5
F35.13	No binding	5	No binding	5
F35.14	No binding	5	No binding	5
F35.15	No binding	5	No binding	5
F35.16	No binding	5	No binding	5

Table 3: pK_i values, obtained for compounds originating from differential docking from whole cell binding studies as determined from using ^{3}H-SB674042 (CHO-OX_1 cells) and ^{3}H-EMPA (CHO-OX_2 cells). Values are mean ± sem from n separate experiments. [a]The compound corresponding to F21.1 and F33.1 was found twice in the similarity searches for the parent compounds P21 and P33, respectively. Hence, we report it in both family trees, but count it only once for the hit rate. [b]The compound corresponding to F21.3 and F22.1 was found twice in the similarity searches for the parent compounds P21 and P22, respectively. Hence, we report it in both family trees.

ID	**CHO-OX_1**		**CHO-OX_2**	
	pK_i	**n**	**pK_i**	**n**
S1.1	No binding	5	No binding	5
S1.2	No binding	5	No binding	5
S1.3	No binding	6	No binding	6
S1.4	IC_{50} > 100 µM	5	IC_{50} > 100 µM	5
S1.5	IC_{50} > 100 µM	5	IC_{50} > 100 µM	5
S1.6	4.83 ± 0.04	5	4.64 ± 0.01	5
S1.7	No binding	5	No binding	5
S2.1	No binding	5	No binding	5
S2.2	IC_{50} > 100 µM	5	4.28 ± 0.04	5
S2.3	IC_{50} > 100 µM	5	IC_{50} > 100 µM	5
S2.4	No binding	5	No binding	5
S2.5	No binding	5	No binding	5
S2.6	No binding	5	No binding	5
S2.7	5.38 ± 0.07	5	5.80 ± 0.02	5
S2.8	IC_{50} > 100 µM	5	IC_{50} > 100 µM	5
S2.9	No binding	5	No binding	5
S3.1	No binding	5	No binding	5
S3.2	No binding	5	IC_{50} > 100 µM	5
S3.3	No binding	5	No binding	5
S3.4	IC_{50} > 100 µM	5	4.40 ± 0.08	5
S3.5	4.47 ± 0.10	5	4.56 ± 0.03	5
S3.6	No binding	5	No binding	5
S3.7	IC_{50} > 100 µM	5	IC_{50} > 100 µM	5
S3.8	4.61 ± 0.08	5	4.82 ± 0.06	5
S3.9	No binding	5	No binding	5